

A highly automated system to define the best operating settings of cryogenic calorimeters

**K. Alfonso^c C. Bucci^d L. Canonica^{d,e,1} P. Carniti^{a,b} S. Di Domizio^{f,g} A. Giachero^{a,b}
C. Gotti^{a,b} L. Marini^{h,i} I. Nutini^{a,b,2} G. Pessina^{a,b}**

^a*Dipartimento di Fisica, Università di Milano-Bicocca, Milano I-20126, Italy*

^b*INFN – Sezione di Milano Bicocca, Milano I-20126, Italy*

^c*Department of Physics and Astronomy, University of California, Los Angeles, CA 90095, USA*

^d*INFN – Laboratori Nazionali del Gran Sasso, Assergi (L'Aquila) I-67100, Italy*

^e*Massachusetts Institute of Technology, Cambridge, MA 02139, USA*

^f*Dipartimento di Fisica, Università di Genova, Genova I-16146, Italy*

^g*INFN – Sezione di Genova, Genova I-16146, Italy*

^h*Department of Physics, University of California, Berkeley, CA 94720, USA*

ⁱ*Nuclear Science Division, Lawrence Berkeley National Laboratory, Berkeley, CA 94720, USA*

E-mail: irene.nutini@mib.infn.it

ABSTRACT: Cryogenic macro-calorimeters instrumented with NTD thermistors have been developed since several decades. The choice of NTD bias current is crucial for the optimal operation of this type of detector. The CUORE detector, consisting of an array of 988 TeO₂ crystals, coupled with NTD-Ge thermistors, and operated at ~10 mK, utilizes this technology. New automatic procedures for the characterization and optimization of the detector parameters were developed for CUORE in order to address the large number of calorimeters and the intrinsic spread of their characteristics, reaching optimal signal to noise ratio and linear response for each detector.

KEYWORDS: keywords

¹currently at Max-Planck-Institut für Physik, D-80805 München, Germany

²Corresponding author.

Contents

1	Introduction	1
2	NTDs characterization and working points	2
3	Performing characterization measurements	5
3.1	Electronics	6
3.2	DAQ	7
3.3	Measurement procedure	9
4	Optimal working points in CUORE	11
4.1	From raw-data to characterization plots	11
4.2	Identification of the optimal working point	12
4.3	Detector response at the optimal working point	15
4.4	Measurements at different temperatures	16
5	Conclusions	17

1 Introduction

Cryogenic calorimeters, also called bolometers, represent one of the leading techniques for rare event searches. This class of low temperature detectors features an excellent energy resolution, sensitivity to all kinds of particles, low energy threshold, and a wide choice of absorber materials [1]. At present, the largest implementation of the bolometric technique is the CUORE experiment, designed, constructed and operated to search for ^{130}Te neutrinoless double beta decay ($0\nu\beta\beta$) [2]. The CUORE detector consists of an array of 988 TeO_2 crystals operated as cryogenic calorimeters at ~ 10 mK. The crystals are $5\times 5\times 5$ cm³ each and weigh an average of 750 g; thus the total detector experimental mass almost reaches the ton-scale. Each TeO_2 crystal, operating as an energy absorber, is instrumented with a Neutron Transmutation Doped germanium (NTD-Ge) thermistor, acting as a phonon sensor, and a silicon heater to periodically inject a fixed amount of energy to the detector for gain stabilization [3–5].

The NTD thermistor converts the thermal phonons, produced by any energy release in the TeO_2 crystals, into a measurable resistance variation that is proportional to the total energy of the collected phonons. The resistance variation can be read out by applying a bias current to the sensor and thus converting it to a voltage variation. The choice of the value of the NTD bias current is crucial for the optimal operation of the detectors.

The behaviour of the detector with respect to the applied bias is described by the characteristic I-V curve. The I-V curve measurement and the identification of the optimal bias current, or *optimal working point* (optimal WP), is a standard procedure for the operation of cryogenic calorimeters.

CUORE's predecessor experiments (i.e. MiDBD, Cuoricino, CUORE-0)[6] had all a small number of detectors and the optimization was handled manually by changing the parameters of the bias circuit and measuring the resulting voltage output with a standard oscilloscope, or data acquisition system. In CUORE, the large number of calorimeters and the intrinsic spread of their characteristics obliged to develop new automatic procedures for the characterization and optimization of various detector parameters [7–9]. The automatic procedure for the identification of the optimal WP permits faster and more precise measurements, resulting in better control over the detectors performance. In addition, it has also been the first time in which the optimal working points were identified by a dedicated algorithm which takes into consideration not only the I-V curve and the voltage amplitude, but also the signal-to-noise ratio and the pulse shape variation with the bias current.

In the following we will describe the procedure for measuring the NTD characteristic curves and for identifying the optimal working point. We will first introduce the working principle of the NTD and the parameters that play major roles in the characterization of these devices and in the construction of the load curves. We will give an overview of the hardware and slow control software, with which the data from the CUORE detectors are controlled and acquired. Lastly we will provide a detailed description of the aforementioned procedures for characterizing the NTDs and of the developed analysis algorithms for identifying the optimal working point.

The procedures described in this paper were applied to the CUORE and CUPID-0 experiments, setting the foundation for the scientific results they obtained [10–17]. The same automated system can be applied to any array of cryogenic calorimeters read by NTDs, such as CUPID [18], easing the procedures for detector characterization and optimization.

2 NTDs characterization and working points

The NTD-thermistor converts thermal pulses into electrical signals through a resistance variation. The NTD-thermistors are usually germanium semiconductor slabs doped by means of thermal neutrons [19, 20]. When the doping concentration reaches a critical value, the NTD enters the metal-insulator transition (MIT) region, where its resistivity exhibits a strong dependence on the temperature [21]. At sub-Kelvin temperature, the thermistor resistance dependence on the temperature is described by [22]:

$$R(T) = R_0 \exp\left(\frac{T_0}{T}\right)^\gamma \quad (2.1)$$

where R is the thermistor resistance, R_0 and T_0 depend on the doping concentration and on the geometry, T is the temperature, and the γ exponent depends on the conduction mechanism. The parameters R_0 , T_0 and γ are usually determined using measurements of the thermistor resistance at various temperatures. For CUORE-like NTDs (with dimensions of $3 \times 3 \times 1 \text{ mm}^3$ ¹), typical values are: $R_0 = 1.0 - 1.5 \text{ } \Omega$, $T_0 = 4.0 - 5.0 \text{ K}$, and $\gamma \simeq 0.5$ [3]. At $T \sim 10 \text{ mK}$, typical resistance values for CUORE-like NTDs are of the order of a few hundred $\text{M}\Omega$ such that an energy deposition of 1 MeV in the absorber induces a resistance variation of a few $\text{M}\Omega$.

¹The small size of the NTD compared to the crystals allows to have a small contribution to the detector heat capacitance, while ensuring good electrical properties in terms of resistance value.

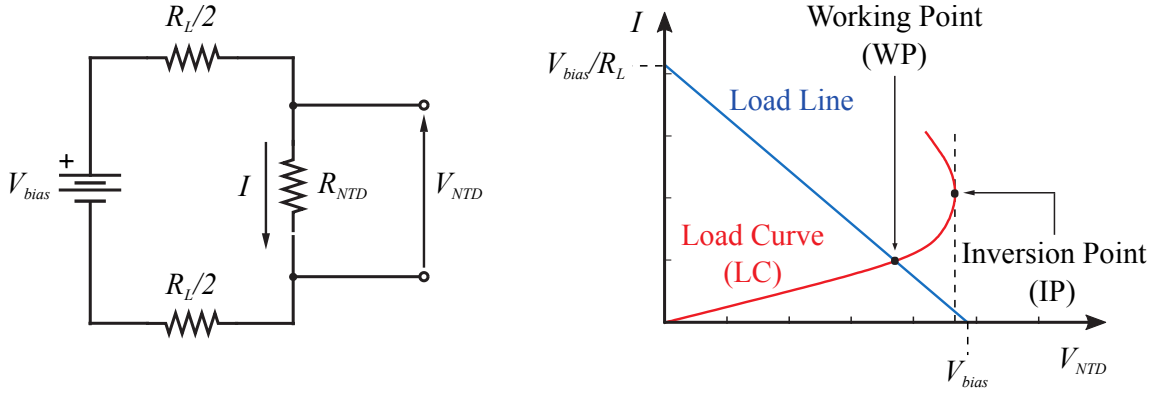


Figure 1. [Left] Scheme of the biasing circuit for the thermistor readout; R_{NTD} corresponds to the NTD resistance R . [Right] Load curve (I-V) of an NTD, an analytical example.

To measure the NTD resistance and its variation, the sensor is biased with the circuit schematically represented in Fig.1[left]. A bias voltage V_{bias} , produced by a dedicated circuit, is applied across a pair of load resistors $R_L/2$, in series with the thermistor. The total resistance R_L is chosen much higher than the thermistor resistance R , so that the current I flowing through the thermistor can be considered approximately constant. The voltage across the thermistor and the power dissipation produced by the current I flowing through the NTD are:

$$V_{NTD} = I \cdot R(T) \quad , \quad P = I \cdot V_{NTD} \quad (2.2)$$

The thermistor temperature T is affected by the power dissipation P : $T = T_b + \frac{P}{G}$, where the base temperature T_b , is the temperature of the heat sink and G is the conductance between the NTD and the heat sink. For high power dissipation, the increase in the thermistor temperature P/G , is comparable to T_b and is not negligible. The power dissipation acts back on the NTD, decreasing its resistance since it varies with the temperature of the device. This phenomenon is called *electro-thermal feedback* and it is valid whenever the load impedance, either static or dynamic, is larger than that of the thermistor impedance, see also below.

The I-V curve for semiconductor thermistors is usually referred to as the *current-voltage characteristic curve*, or *load curve*. An example of a load curve (LC) is shown in Fig.1[right]. Given a fixed base temperature, the slope of the load curve is nearly constant for low I . When the bias current is sufficiently high, the electro-thermal feedback causes the I-V relation to deviate from linearity leading to a non-ohmic behavior; beyond the “inversion point” (IP), the slope becomes negative. Within the ohmic region, each point on the load curve is associated with a *static resistance* of the NTD.

Each point on the I-V curve is a potential *working point* (WP). As shown in Fig.1[right], WP is the point of intersection between the load line ($V_{NTD} = V_{bias} - I \cdot R_L$), which translates with V_{bias} , and the load curve. We change the NTD bias current, in order to find the detector’s best operating conditions along the I-V curve, the optimal WP.

The procedure for determining the optimal WP consists of monitoring the amplitude of a pulse of fixed energy while varying the bias current, and finding the point where the signal to noise ratio

is maximum. For this reason, not only does the amplitude of the signal pulses play an important role in the choice of optimal WP, but also the noise.

An estimate of the noise level of the detector is evaluated from the analysis of the baseline fluctuations. In CUORE the resistance range of NTDs is large and the series noise of the amplifier is negligible; the intrinsic noise is dominated by the parallel Johnson noise of the load resistances across the impedance of the thermistor. The noise spectral density of the NTD voltage, in worst condition, is proportional to the NTD resistance and to the temperature of both the thermistor and the load resistors: $\Delta V_{NTD}^2 \propto \frac{R^2}{R_L} \frac{T_L}{T}$, with $T \sim 10$ mK and $T_L \sim 300$ K (room temperature) in our case. For cryogenic calorimeters, given an energy release in the absorber, the thermistor resistance varies, leading to a signal pulse. The NTD pulses for a given energy deposition are quite small, $\Delta V_{NTD} \sim 100 - 400 \mu\text{V/MeV}$; the signals require amplification. The average voltage read after the amplification stage (V_{bsl}) is used to reconstruct the NTD voltage (V_{NTD}) since they are related by:

$$V_{bsl}^{\pm} = A_V \cdot (V_{off} \pm V_{NTD}) \quad (2.3)$$

where V_{off} is the residual input-referred offset of the electronics, A_V is the gain of the amplification stage, and the \pm sign corresponds to the bias polarity. Moreover, for signal pulses, the relationship between the maximum voltage variation (or pulse amplitude), A , and the energy deposition resulting in a temperature variation, ΔT , is $A \propto \frac{\Delta T}{T} V_{NTD}$; this dependence holds if the thermistor logarithmic sensitivity [23] is used to correlate resistance and temperature variations. The signal amplitude increases with V_{NTD} , increasing the bias. However the increase of the applied bias voltage results in an higher temperature and lowers the $\Delta T/T$ ratio, therefore the A vs V_{bias} curve will reach a maximum and then will start decreasing.

The electro-thermal feedback also has an effect on the pulse shape; the non-ohmic behavior of the device for high bias current leads to instabilities in its dynamic response, resulting in distorted pulses or in an oscillation of the detector. In order to avoid regenerative electro-thermal feedback, semiconductor thermistors should not be loaded with an impedance smaller than the impedance of the thermistor itself. In CUORE, the NTDs are read out by an amplifier at room temperature and this leads to a large parasitic capacitance of the link in parallel to the NTD. This capacitance gives the dominant contribution to the load impedance in the bandwidth of interest.

At low bias, the NTD impedance is purely resistive and equals the ratio of its bias voltage and current: in this case an oscillation can start if the signal has a frequency content for which the module of the parasitic capacitance becomes smaller than that of the thermistor impedance. The feedback, however, increases the power and the NTD thermistor lowers its resistance, damping the oscillation (i.e. the NTD impedance is real).

At high bias, moving towards the inversion point, the NTD thermistor deviates from the resistive regime and its dynamic impedance shows an inductive component: in this case, when the inductive component gets sufficiently high, the oscillation is maintained instead of being damped [24]. This region of operation must be avoided in order to have a stable detector operation.

In order to measure the pulse amplitude (A) and shape variation with bias voltage, a reference energy injection is needed. For this purpose, either a line from a reliable radioactive source, or a given power injection from the heater installed on the crystal, could be used. Generally, the latter solution is chosen because of the higher precision of the energy injection and the possibility of regulating the rate of heater pulses for each NTD bias configuration.

In conclusion, the optimal WP is chosen as a compromise between having a large SNR and ensuring a stable and linear behavior of the NTD, which is crucial for the best operation of the thermal sensor.

Despite the previous considerations, in real experimental conditions, we do not have ‘a priori’ knowledge of all the NTD parameters and conductances. Moreover there can be further contributions to the noise related to vibrations, pick-up noise, etc. Therefore the NTD optimal working point must be determined experimentally and dedicated measurements on the NTDs are necessary. Three types of measurements, which we will refer to as *characterization measurements*, can be performed:

- *Load curve measurement*: accurately reconstruct the current-voltage (I-V) curve, in order to characterize the NTD static behavior and identify the range of bias voltages for which the pulse amplitude is close to its maximum;
- *Working point measurement*: accurately build the signal-to-noise ratio (SNR) curve and study the pulse shape variation as a function of the applied bias voltage in order to find the optimal WP;
- *Resistance measurement*: precisely measure the NTD static resistance at a given bias voltage to monitor its stability over time.

Estimators for the NTD resistance, voltage variation for a given energy deposition, and noise are therefore calculated for each different bias current value from the mentioned measurements. The procedures and algorithms used to reconstruct the NTD’s voltage/current/resistance (V_{NTD} , I , R), noise (N), pulse amplitude (A), signal-to-noise ratio (SNR) will be described in detail in Sec.4.

3 Performing characterization measurements

A dedicated procedure has been developed in order to perform *characterization measurements* of the response parameters for each of the 988 CUORE detectors. Since no NTD- TeO_2 system is exactly the same, it is necessary to optimize each crystal’s NTD bias voltage from the analysis of the *load curve* data.

In the following, we will first present the CUORE electronics systems for the readout of the NTD-Ge thermistor (R_{NTD}) and for power injection through a Si heater (R_{heat}), as represented in Fig.2. We will focus on the design specifications of the CUORE front-end boards, utilized for the NTD biasing circuit (introduced in Sec.2) and amplification stage, and the capabilities of the pulser board. Next, the function of the CUORE data acquisition system (DAQ) to identify and associate raw data from the detector with designated electronics settings will be discussed in relation to the *characterization measurements* on the NTDs from Sec.2. Lastly, we will describe the load curve measurement, including the front-end and DAQ configurations for the procedure. We emphasize the design considerations of each infrastructure to facilitate the operation of a large array of cryogenic detectors.

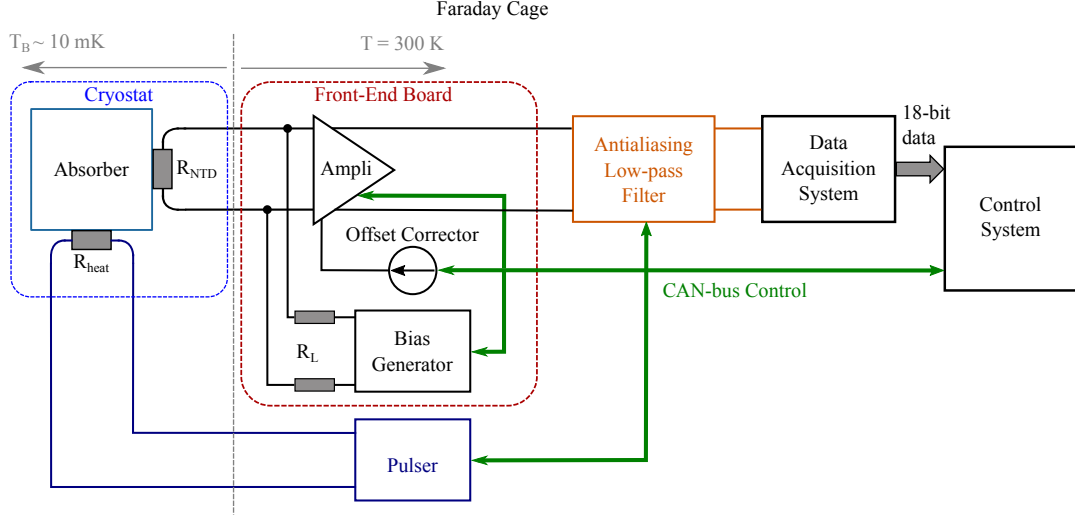


Figure 2. Schematic of the CUORE detectors electronics and DAQ chain.

3.1 Electronics

The front-end electronics system, specifically developed for the CUORE experiment, is responsible for the differential signal amplification, detector biasing, and detector thermal response calibration and stabilization. The first two functions are performed by the JFET-input preamplifier and the front-end board [25], while the calibration is handled by the pulser board [26]. Auxiliary electronics systems provide anti-aliasing filtering [27], power supply regulation, and high-stability voltage references [28, 29]. The technical details of these electronics systems are described thoroughly in the references provided above; in the following we will mainly highlight the characteristics that influence any *characterization measurement* (load curves, working point measurement, etc.).

The detector bias current is generated by applying an adjustable differential voltage to two alternative pairs of high-value custom-made load resistors placed at room temperature, which have a designated value of $60\text{ G}\Omega$ ($2 \times 30\text{ G}\Omega$) or $10\text{ G}\Omega$ ($2 \times 5\text{ G}\Omega$). For this reason, in the following sections we use the term bias voltage instead of bias current. The resistor value selection is done through relays, whose layout was optimized to avoid thermal drifts of the bias current [25]. Having two possible values for the load resistors enables proper readout of a broad range of detector impedance, from a few hundred $\text{k}\Omega$ up to a few $\text{G}\Omega$.

The bias voltage has a maximum differential range of $\pm 50\text{ V}$, which corresponds to 0.8 nA (5 nA) bias current with $30\text{ G}\Omega$ ($5\text{ G}\Omega$) load resistors, a resolution of 16 bits, and a thermal drift better than $80\text{ ppm}/^\circ\text{C}$. Each of the two differential voltages (positive and negative) can be set independently from the other, providing the capability of applying a bias voltage with non-zero common-mode voltage. This is useful when evaluating and optimizing the DC common-mode rejection ratio (CMRR) of the preamplifiers, which is important for suppressing any common-mode noise source; internal trimmers are used for optimizing the CMRR. Once the bias voltage is set by the on-board circuitry, a relay is used to invert the polarity of the bias applied to the detector without further adjustments. This operation provides the capability of taking the difference between the two configurations (direct and inverted bias), thus canceling purely electrical offsets due to the

Signal amplification	Fully differential
Input transistors	InterFET NJ132 (custom pairs)
Gain settings	20 V/V – 10k V/V
Gain stability	< 5 ppm/°C
Offset adjustment	±80 mV
Offset stability	< 1 μ V/°C
Input bias current	< 100 fA
Input differential current	< 20 fA
Series noise	3.3 nV/ $\sqrt{\text{Hz}}$ (white) 8 nV/ $\sqrt{\text{Hz}}$ (1 Hz)
Parallel noise	< 0.15 fA/ $\sqrt{\text{Hz}}$
CMRR (after optimization)	> 120 dB
Bias voltage (V_{bias}) range	±50 V
Load resistors (R_L)	$2 \times 30 \text{ G}\Omega$ or $2 \times 5 \text{ G}\Omega$
Bias current range	±0.8 nA @ 60 G Ω , ±5 nA @ 10 G Ω
Bias voltage resolution	16 bits

Table 1. Summary of the front-end electronics specifications.

preamplifier voltage offset. In the case when the load curves are acquired with a single polarity, the effect of the offset can be minimized by adjusting it to zero before performing the measurements. Thanks to the proper custom design, the JFETs' gate current (below 20 fA differential and below 100 fA single-ended) is completely negligible with detector impedance up to a few G Ω [30]. If the gate current were not negligible, its residual power injection could still be taken into account [31].

The signal amplification is fully differential and the gain is remotely programmable (from 20 V/V up to 10k V/V) in order to accommodate the broad dynamic range of this type of detector when it is operated at different base temperatures. The offset can be digitally adjusted up to ±80 mV (input-referred) and its stability is calibrated to be better than 1 μ V/°C, enabling reliable baseline monitoring even for very long operating times (years).

Detector thermal response stabilization is performed using a pulser board that is capable of applying precise (sub ppm/°C), low-noise voltage pulses to a Si heater resistor glued to the detector. The response of the detector to such a heat pulse enables the monitoring of the detector behavior at different base temperatures and bias currents.

All the adjustments done by the front-end electronics (bias voltage, relay switching, offset adjustment, pulse generation, etc.) are managed by the on-board firmware. In this way, each operation can be easily parallelized since the DAQ provides only a few slow control commands to the front-end electronics through the CAN bus interface, while all the computation algorithms are managed by the on-board microcontrollers.

Table 1 summarizes the specifications and characteristics of the front-end systems.

3.2 DAQ

The CUORE data acquisition system, described in detail in [32], consists of a core system for data digitization and storage, and of a control interface for the analog electronic readout chain. The

detector waveforms are acquired with a 1 kHz sampling frequency by a 18-bit ADC. The relatively low signal bandwidth (on the order of 10 Hz) makes it possible to digitize and save the continuous waveforms of the detectors for offline processing. For the same reason, triggering can be performed in software, allowing for more flexibility and control. The data analysis is performed on triggered events, namely finite-length waveform windows selected in correspondence of a trigger. The default event window length used in CUORE is 10 s. Events are associated with supplementary information including *DetectorId* (an identifier which maps the different detectors in the CUORE array), time, and the type of trigger that caused the generation of the event. Three types of events exist: *signal events*, generated when the signal trigger detects a pulse in the waveform; *noise events*, generated periodically or at a random time, regardless of the presence of a pulse in the waveform; and *pulser events*, whose generation is forced in correspondence to the injection of a pulse from a heater attached to the absorber.

The control software for interfacing with the analog electronics is implemented with a multi-threading approach, allowing concurrent communication with multiple target a single CAN bus link. Some digital signals are acquired synchronously with the waveforms from the calorimeters and are used to synchronize external events with the data. In particular, digital signals are generated in correspondence to changes in the electronics configuration and when pulser-generated signals are injected in the detectors. The synchronization mechanism enables pulser-generated events to be identified and flagged in the offline analysis. Similarly, each acquired event can be associated with an *EleId*, i.e. an identifier for a well-defined electronics configuration (which includes parameters like V_{bias} , R_L and A_V). This capability of characterizing the measurement procedure is fundamental for the offline analysis because it enables events to be classified based on their *EleId*.

Depending on the goal of the particular measurement being performed, one or more of the following quantities are estimated for each electronics configuration and for each detector: the steady-state baseline voltage, the noise power spectrum, and the parameters of the detector response in presence of pulses. As discussed in Sec.2, these quantities are used to estimate the values of the detector parameters that help determine the optimal configuration of the NTDs. Quantities related to the steady-state performance of the detector are estimated from the noise events, while quantities related to the detector response in presence of pulses are estimated from pulser events. The pulser-based approach enables control over the timing and amplitude of the heat-injected pulses and avoids relying on the trigger settings, which would need to adapt for any change in the electronics configuration.

From a procedural point of view, any *characterization measurement* consists of applying a sequence of electronics settings to the detectors, and to acquire, for each of these configurations, n noise events and p pulser events. All the following data processing is left to the offline analysis, see Sec.4. The configurable numbers n and p of noise and pulser events are usually chosen larger than one, so that events that do not pass quality cuts can be discarded in the analysis, and the estimated quantities can be averaged over multiple events.

The *characterization measurements* introduced in Sec.2 are implemented as:

- *Load curve measurement.* In the current-voltage (I-V) curve, both positive and negative bias polarity configurations are measured for a large range of bias voltage values. In this case, the main purpose is to measure the thermistor voltage as a function of the bias current. An

example of the detector output for this type of measurement is reported in Fig.3.

- *Working point measurement.* In the signal-to-noise ratio (SNR) curve, only unipolar bias configurations (e.g. negative) are measured for a sub-range of bias voltage values. The bias voltage values are concentrated around the maximum of the pulse amplitude identified in the I-V curve. A large number of noise and pulser events, much more than those taken during the *load curve measurement*, are acquired in order to improve the accuracy of the measurement. The preamplifier output is offset, such that we can maximize the signal gain of the readout chain for the negative polarity configurations. In this way, we can fully exploit the digitizer ADC dynamic range, increasing the precision in the reconstruction of all the pulse-related parameters.
- *Resistance measurement.* The NTD resistance value for a given applied bias voltage is obtained from measuring a single point of the I-V curve in the linear region. The NTDs voltage, current (and resistance) are obtained from two configurations with opposite polarity and the same bias voltage, which is usually the one chosen for physics measurements.

All these *characterization measurements* are usually performed in parallel on a large number of detectors. Their duration is determined by the number of electronics configurations, the number of noise and pulser events acquired for each configuration, and by the time needed for the detectors to stabilize after an electronics configuration is applied. For example a resistance measurement performed in parallel over all the CUORE detectors lasts about 3 hours, while an I-V curve measurement performed over 3 CUORE towers takes about 12 hours.

3.3 Measurement procedure

The three *characterization measurements* introduced in Sec.2 and in Sec.3.2, share a similar dedicated sequence in the data acquisition, whose procedure is illustrated in the following. This sequence has been specifically designed to measure the characteristic parameters for each of the CUORE detectors, but can also be adapted to any cryogenic macro-calorimetric experiment using NTDs as phonon sensors.

The *load curve measurement* is the most general procedure since it is partially comprised of the working point and resistance measurement procedures. The first step consists of adjusting the preamplifier gain and offset in order to exploit, at best, the entire ADC dynamic range to avoid saturation and to ensure that, during the measurement, the output signal takes values in a range almost symmetric around zero.

Each load curve point, identified by an `EleId`, is set by applying the required bias voltage at negative bias polarity, waiting some time to reach a steady output, and acquiring the baseline voltage for the chosen number of noise/pulser events. Bias polarity is then inverted and the measurement is repeated.

The purpose of measuring the output signal at both positive and negative bias voltage polarity is to cancel the contribution of the residual input offset when measuring the average value of the output signal. Since the only use of positive polarity step is the cancellation of the residual input offset, its duration is determined only by the number of *noise events* required. A reference heater pulse,

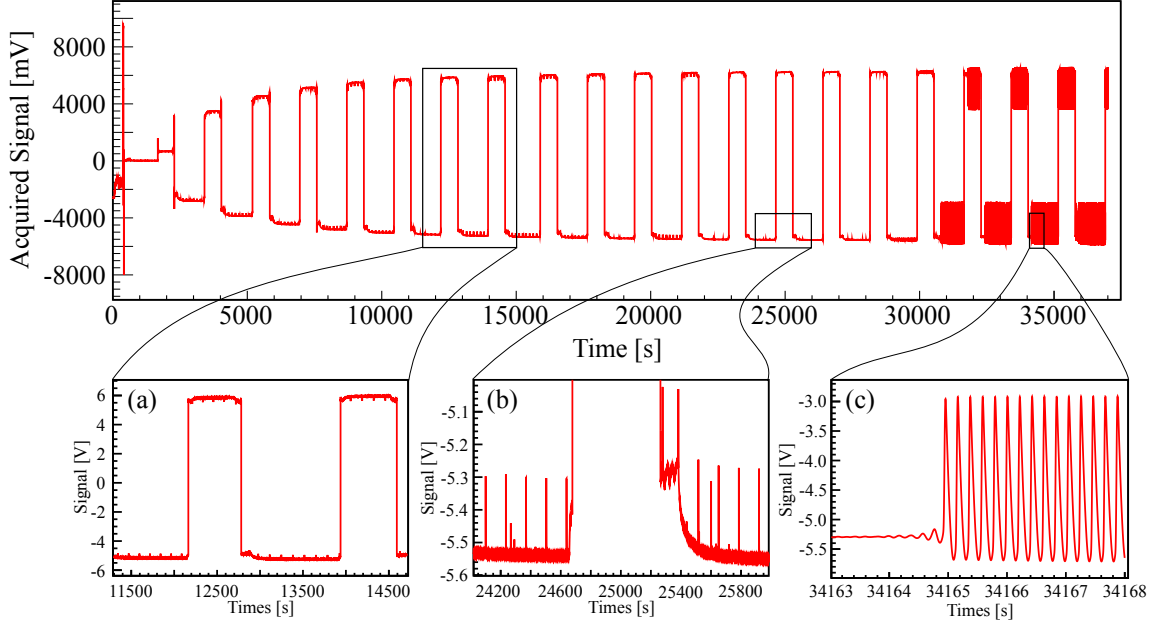


Figure 3. Continuous waveform output during a *Load curve measurement* for one CUORE detector. For each bias configuration, EleId, the data are acquired both for negative and positive polarity. In zoom (a), we see two different bias configurations, with data taken at negative and positive polarities in which it is clearly visible the baseline inversion. Zoom (b) shows the transient time spent in configuring the electronics, waiting for the detectors to stabilize and for performing the actual measurement for each polarity for a given EleId. In the last high-bias configurations, the detector output is oscillating, as reported in zoom (c).

with fixed energy of ~ 1 MeV, is periodically fired for the entire duration of the measurement. The heater pulse amplitude acts as a reference to monitor the signal to noise ratio, the pulse amplitude, and shape variation for every applied bias voltage. In order to simplify the data reconstruction and analysis, we endorsed to use *pulsar events* from only the negative bias polarity, where each signal is characterized by a fast upward pulse; therefore the duration of each negative polarity step is driven by the number of pulses that are required to obtain a good estimate of their amplitude and shape parameters. Once one point of the load curve is completed, the polarity is switched again to negative and a new higher value of the bias is set (see Fig.3 - zoom (a)). This procedure is repeated with increasing bias voltage, as shown in Fig.3, until a pre-determined maximum bias value is reached. It is worth noting that between each configuration there is a transient region of thermal origin, as shown in Fig.3 (b). Writing any electronics parameter, and in particular changing the bias voltage value, has a thermal effect on the output signal which can last up to a few hundreds of seconds. This region is not assigned to any valid EleId in order to discard corresponding events in the reconstruction and analysis phases.

The maximum bias is set just below the point a prompt oscillation starts. An example of the oscillating effect described in Sec.2 is shown in the bottom right insertion of Fig.3 (c). The values of the maximum bias voltage for each NTD are specified in a configuration file. Similarly, the number of steps, the duration of each step, the number of pulses in the negative polarity and the number of *noise events* to be acquired in the positive polarity, are all specified in a configuration

file, making the procedure flexible and easy to adapt to the different *characterization measurements*. For each EleId, the typical number of *noise events* is between 5 and 15, while the typical number of *pulsers events* is between 10 and 30, depending on the required accuracy.

4 Optimal working points in CUORE

In the following, we will discuss the procedures to construct the load curves and derive the relevant parameters for the selection of the optimal WP, namely pulse amplitude (A), noise (N), and signal-to-noise ratio (SNR).

We emphasize the new analysis techniques, accounting for pulse-shape quality checks to identify good detector operating conditions, as a crucial consideration in selecting the WP. Moreover, a regular monitoring of NTD resistance during the data-taking ensures the detectors are operating in a stable condition. All data shown in the first parts of this section were acquired by CUORE at a base temperature of 11.8 mK.

This section concludes with a discussion of the characterization procedures applied to a wide range of temperatures, further demonstrating their versatility. The study of the temperature dependence of the detector parameters is important to model and optimize their response.

4.1 From raw-data to characterization plots

Once a *characterization measurement* has been acquired, the reconstruction of the raw data is performed through a sequence of event-based analysis modules [33].

The goal of the reconstruction software is to obtain all the parameters (V_{NTD} , SNR, A and N) as a function of the NTD current I , for each point of the load curve measurement (EleId). The analysis steps necessary to compute the above mentioned parameters are repeated for each pair of EleId with similar electronics configuration: same bias current, but opposite polarity. In this section, we plot V_{NTD} as a function of I instead of the canonical way to represent the load curve (see Fig.1), in order to coalign the related (independent) variables on the horizontal axes with respect to the curves for the A, N and SNR variables. In Fig.4, there is an example for each of the curves built for a single NTD sensor. These curves are used to determine the configuration that maximizes the pulse amplitude while minimizing the noise level, thus to select the optimal working point.

In order to compensate for the effects of the electronics offset, the NTD voltage V_{NTD} is calculated as:

$$V_{NTD} = \frac{V_{bsl}^+ - V_{bsl}^-}{2 \cdot A_V} \quad (4.1)$$

while the current is:

$$I = \frac{V_{bias} - V_{NTD}}{2 \cdot R_L} \quad (4.2)$$

where V_{bsl}^\pm is the baseline value, read at the amplifier output and scaled by the voltage gain, at each polarity for a given EleId, as reported in Eq.2.3.

Accordingly, each NTD resistance is obtained from the ratio of V_{NTD} and I .

The reconstruction software aims to compute event-based variables and to select a clean sample of events, where *clean sample* refers to events that do not show drifting output signal, particle induced pile-up, etc.

V_{bsl}^+ and V_{bsl}^- are obtained directly from clean samples of *noise events*. V_{NTD} is then calculated using the EleId parameters (A_V , R_L and V_{bias}). Similarly, the signal noise N and the pulse amplitude A are obtained from a clean sample of *noise events* and *pulser events*, respectively.

Among the variables computed from the waveform of the *noise events*, the most important are the baseline and the noise. The baseline is defined as the average waveform value evaluated from a linear fit of the samples in the event window. All the baseline values of events with the same EleId-NTD are averaged, in order to obtain each time a unique value for V_{bsl}^\pm . The noise level of each configuration is evaluated exploiting the optimum filter [34]. N is therefore computed as the integral of the noise power spectrum of each *noise event*, weighting each frequency based on its contribution to the average pulse, resulting in the resolution of the optimum filter. An alternative and simpler method consists of computing for each *noise event* the standard deviation of the NTD output samples; the average of these values is taken as N for each EleId-NTD. We preferred to use the first method, although more complicated, since it suppresses frequencies irrelevant to the detector signal bandwidth.

The *pulser events* are employed to compute the amplitude of each heater pulse and a number of pulse-shape parameters used as indicators of possible distortion of the pulse itself. The detailed description of the distortion indicator is provided in Sec.4.2. The amplitude of a pulse is usually defined as the difference between the maximum of the pulse and the baseline value in the region before the trigger. Instead of evaluating this quantity for each *pulser event* and defining the amplitude estimator A as the amplitudes average, we directly average all the *pulser event* waveforms and define A as the amplitude of the averaged pulse. This allows to reduce the effect of incoherent noise.

Eventually, the signal to noise ratio SNR is computed as the ratio of the amplitude and noise estimator.

4.2 Identification of the optimal working point

From the analysis of the curves constructed for each detector in a *working point measurement*, the optimal WP is chosen following two basic requirements: maximize the signal to noise ratio and avoid pulse deformation. An automated algorithm was developed to find the optimal bias voltage for each detector.

The shape of the heater pulses at the different bias voltages has been investigated as a figure of merit for identifying unstable conditions, which could appear when the NTD is operated in the non-ohmic regime.

The detector response is modeled with an empirical function whose Laplace transform has 4 real negative poles and one negative zero in the complex plane, and the pulse is considered as distorted if a pair of poles departs significantly from the real axis, becoming complex conjugate [35].

A fit of the heater pulses with the empirical template is performed and a global shape parameter S is constructed from the fit results. Given a pole P in the complex plane, the parameter S is defined as

$$S = \frac{|Im(P)| - |Re(P)|}{|P|} \quad (4.3)$$

and its value changes with the applied bias voltage; this is correlated with the ability to reconstruct and predict the pulse deformation.

For low bias values, the pulse shape is well-described by one time constant on the rising edge and

Bias Voltage (V_{bias})	1.8 V	2.4 V	3.8 V
Pulse Amplitude (A)	0.148 V	0.144 V	0.130 V
Signal-to-noise Ratio (SNR)	300 mV/mV	330 mV/mV	360 mV/mV
Shape parameter (S)	-0.35	-0.20	0.05

Table 2. Summary of the parameters for the three LC configurations identified by the three pulses in Fig.5.

three time constants on the falling edge, thus the 4 real poles detector response model is satisfactory and the parameter S is negative. Increasing the applied bias, the non-linear effects from the electro-thermal feedback start to be relevant and the pulse starts showing a damped-oscillation shape. These configurations are characterized by a positive value of S , meaning the value of the imaginary term of the pair of complex conjugate poles of the detector response function is higher than its real term, thus the oscillatory part will dominate the shape of the falling edge of the pulse.

When the configuration corresponding to the maximum of SNR is in a region of high bias, the pulse shape can become slightly deformed. A threshold on the S parameter can then be set to identify bias configurations leading to deformed pulses. The threshold is typically around $S = 0$, however its exact value can be optimized based on the specific experimental configuration and can be slightly different for measurements at different base temperatures. For CUORE data at 11.8 mK, the threshold is set as $S \leq -0.2$.

If the maximum SNR corresponds to non ideal pulses, the algorithm iteratively takes the previous points on the load curve and applies the same shape checks. Eventually the optimal WP is chosen, among the points with no deformation, as the point with the highest SNR.

Characterization curves produced for one CUORE detector from the *working point measurements* and analyzed in order to find the optimal WP for the NTD are shown in Fig.4. The corresponding heater pulses at three different bias voltages (under-biased, optimal, over-biased) for the same detector are shown with the effective fit superimposed in Fig.5.

In Fig.4, the pulse amplitude reaches its maximum for $V_{bias} = 1.8$ V and has an ideal shape; however the SNR is not maximized in this configuration, due to higher noise RMS for lower bias voltage. On the contrary, the SNR is maximized for $V_{bias} = 3.8$ V; the position of this point on the I-V curve is far from the linear region and the pulse shows a strong damped-oscillation shape. Therefore the working point $V_{bias} = 2.4$ V is chosen as a compromise between having a high SNR and non deformed pulse.

A summary of the parameters (V_{bias} , A, SNR, S) for the three configurations corresponding to the pulses in Fig.5 is reported in Tab.2.

In general, with the addition of the pulse shape condition, the SNR at the chosen WP is only slightly lower than the maximum SNR (see in Tab.2, the SNR difference is $\sim 8\%$). The choice of the WP in a region of linear response of the NTD is as much important as ensuring a high SNR. The former condition is fundamental for the operation of the NTD, since it will allow the device to maintain almost the same dynamic response for different energy depositions in the absorber. A stable dynamic behaviour of the NTD helps in the further data processing, profiting of the Optimal Filtering technique [34], which assumes a uniform pulse template for a wide energy range.

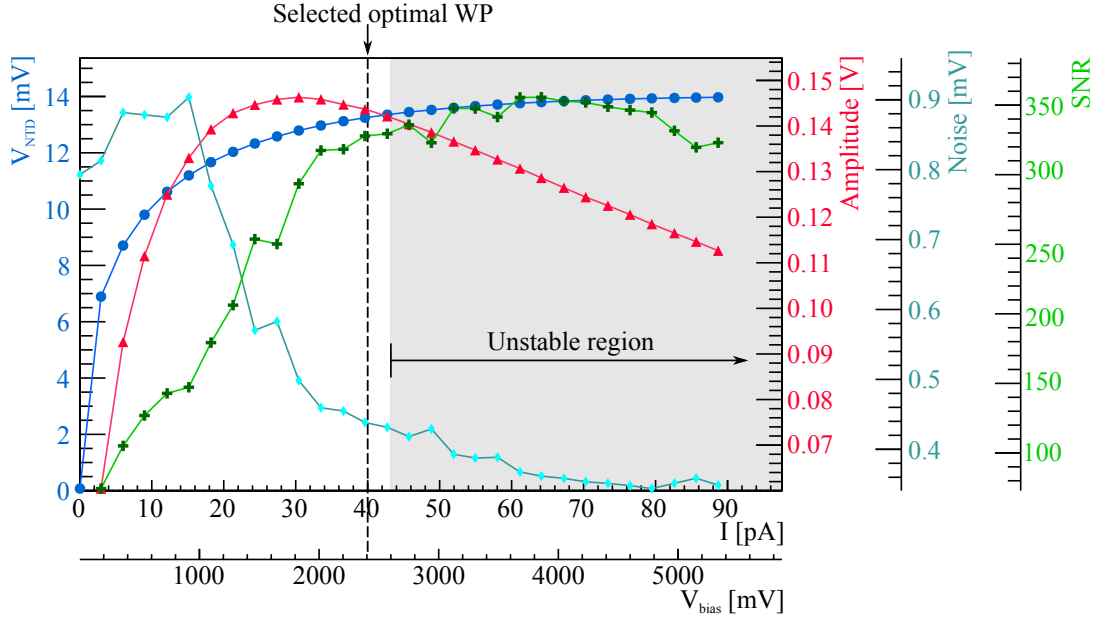


Figure 4. Characterization curves produced in a *working point measurement* for one CUORE detector. The black dashed line indicates the point corresponding to the bias chosen as the optimal WP.

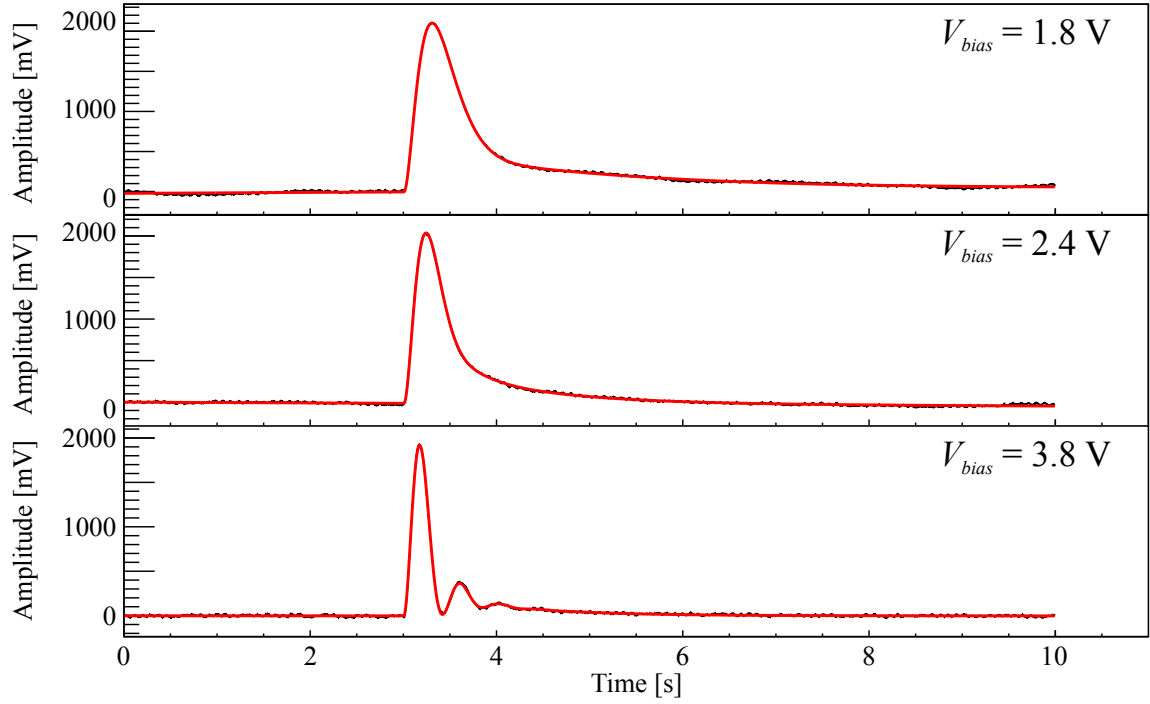


Figure 5. Heater pulses, and their effective fit, for three different bias configurations acquired in the working point measurement, for the same CUORE detector whose I-V, SNR and other plots are reported in Fig.4. [Top] $V_{bias} = 1.8$ V, maximum pulse amplitude. [Center] $V_{bias} = 2.4$ V, selected optimal WP. [Bottom] $V_{bias} = 3.8$ V, maximum SNR. [35]

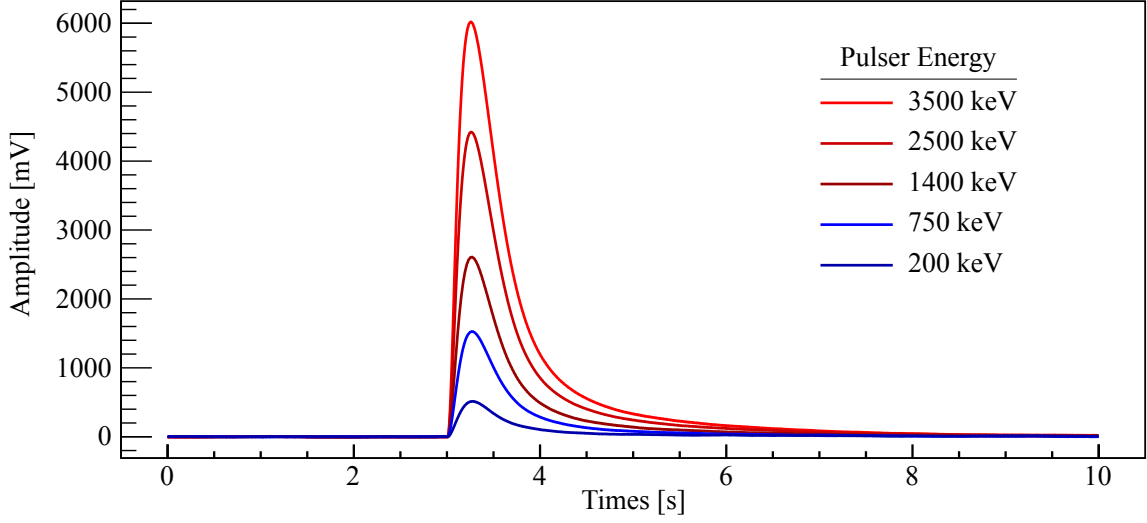


Figure 6. Heater pulses at different energies for the same CUORE detector as in Fig.5, when the NTD is operated at the optimal WP, ensuring the pulse shape to be uniform with energy.

4.3 Detector response at the optimal working point

After setting the optimal working points identified by the algorithm discussed in the section above, a further check of the pulses quality and the stability of the NTD operating conditions is performed.

Dedicated measurements are performed, firing several pulsers of different amplitudes (200 keV - 3.5 MeV). Average pulses for all the different amplitudes are produced for each detector and compared to verify the shape uniformity with energy. A fit of the average pulses is performed with the same template discussed in Sec.4.2 and the global shape parameter S is evaluated. For each detector, if S is consistent among the several energies, the shape uniformity is considered verified. We observed that for approximately 2-5% of the CUORE NTDs the algorithm provides an optimal WP for which the pulse shape slightly changes with energy; these are usually very noisy detectors, for which the evaluation of SNR and shape parameters from a standard load curve measurement are not accurate. For these cases, a tuning of the bias voltages optimal WP is performed manually. Afterwards, another dedicated run with multiple heater pulses is taken, to perform final quality checks on the detectors' pulse shape, especially for those for which the bias has been manually changed and optimized. The final optimal WP ensures a uniform pulse shape at the several pulser energies, see Fig.6.

The optimal WP bias voltage values applied to the CUORE detectors at an operating temperature of 11.8 mK are reported in Fig.7[left]. The values cluster around voltages of 1.5 - 2.0 V. This corresponds to an average WP resistance of $R_{wp} \sim 0.6 - 1.2 \text{ G}\Omega$, see Fig.7[right].

During the standard CUORE data-taking, given an operational temperature and fixed bias voltages, the effective NTD resistance at the optimal WP (R_{wp}) is measured for each detector several times per month, in order to monitor the devices' thermal stability over time; this is the *resistance measurement* described in Sec.3.2. In Fig.8 the stability of the NTD working point resistance for all the detectors during the CUORE data taking at 11.8 mK is reported². Each

²The plot reports the main features of the distributions of the relative variation of R_{wp} for the CUORE detectors

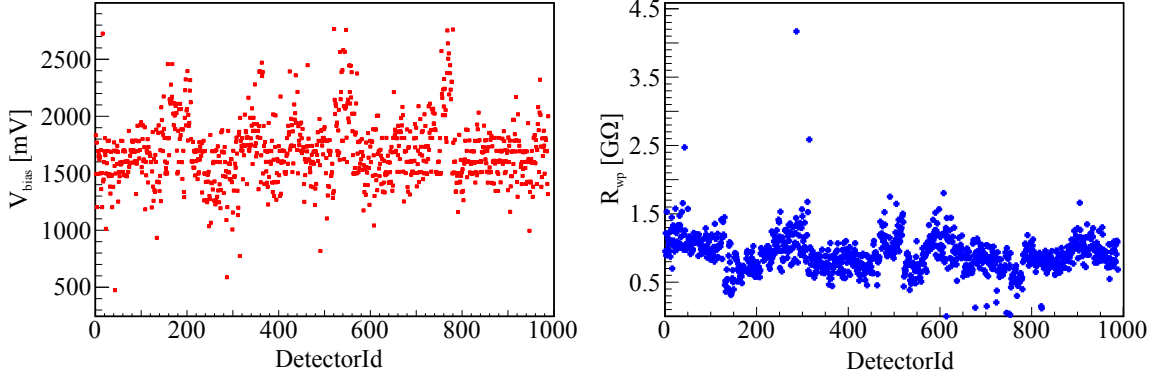


Figure 7. 11.8 mK base temperature. [Left] Distribution of the bias voltages applied to the NTD as a function of the CUORE *DetectorId*. [Right] Distribution of the NTD resistance at the selected WP as a function of the CUORE *DetectorId*.

element in the plot corresponds to the distribution of the relative variation of the values of R_{wp} for the CUORE detectors in two years.

4.4 Measurements at different temperatures

The procedure for characterization measurements and optimal working point identification can be applied at different base temperatures.

A dedicated set of *load curve measurements* from 11 mK to 27 mK base temperature was performed in CUORE. The data were acquired and analyzed with the procedures described above. From the *load curve measurements* at the different temperatures, the variables (V_{NTD} , I , R) at each V_{bias} were calculated. An instructive visualization of the variation at the NTD static behaviour with bias and temperature is provided by the R-P curve (resistance vs. injected power) at the different temperatures, as reported in Fig.9 [Left] for one CUORE detector. These curves show the combined effect of variation of the NTD base resistance with temperature, $R(T|P = 0)$, and its dependence on the power dissipation due to the electro-thermal feedback for increasing bias voltages V_{bias} . Curves with lower base resistance correspond to higher base temperatures. Incidentally, we can see that the minimum bias current used to bias the thermistor is of a few pA, which proves that the effect of the amplifier differential input current of a few tens of fA has a completely negligible effect.

From the analysis of the mentioned *load curve measurements*, we defined a set of optimal WPs for each temperature; these were optimized for each detector-temperature. The variation of the SNR with temperature was then analyzed. Runs with multiple pulser amplitudes (as described in Sec.4.3) were acquired on a subset of CUORE detectors. The SNR was calculated at the different pulser amplitudes. For each pulser amplitude at a given temperature, the average and width of the distribution of SNR values for each detector were evaluated. We observed that the SNR, as well as the optimum filter resolution, improves for lower temperatures. We ascribed this behaviour

measured for each *resistance measurement*. The circle corresponds to the median; the solid box around the median indicates the 50% of the distribution of the data. The dashed lines extending vertically from the boxes indicate the width of 95% of the data distribution.

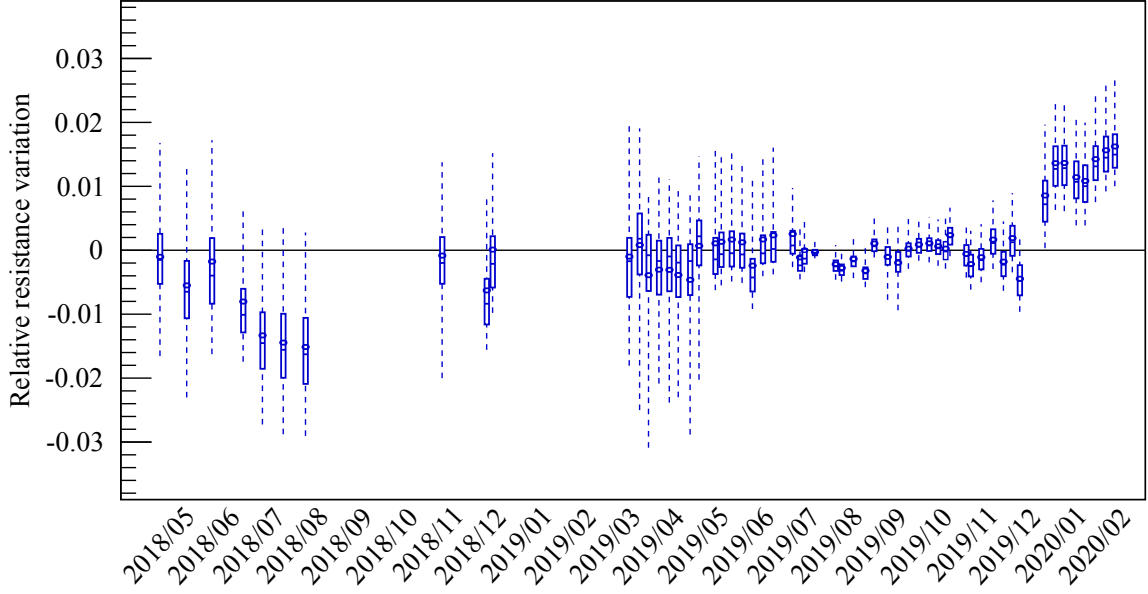


Figure 8. CUORE resistance stability over 2 years operation at 11.8 mK. We evaluate the relative variation with time of the R_{wp} for each single detector compared to a reference measurement (from August 2019). Time intervals with no points correspond to periods of cryogenics maintenance and no data-taking. The data are more spaced in 2018, since *resistance measurements* were performed bi-weekly or monthly. Since 2019, we performed *resistance measurements* once a week and this allows for a continuous and more accurate monitoring of the thermal stability of the detectors and the overall system. The average resistance variation differs for the data of late 2019 and early 2020 and that is correlated with a slight change in the operating temperature; since the applied bias voltages on the NTDs have been always the same, a colder temperature lead to larger values of the NTD resistance.

to the larger absorber internal gain³ for lower temperatures, which over-compensates the increase in the noise RMS due to larger NTD resistance values. An example of the SNR variation with temperature, evaluated as the ratio of the amplitude of the higher pulser (at ~ 3.5 MeV) over noise RMS, is reported in Fig.9[Right].

Thanks to this study it was possible to identify the best operating temperature of the CUORE setup, for which we have then evaluated the optimal WP for each detector. A more detailed discussion on the CUORE temperature studies and detectors thermal response optimization will be part of a future dedicated paper.

5 Conclusions

In conclusion, a dedicated procedure for performing automatic load curve measurements on a large number of cryogenic calorimeters read by NTDs has been developed. The specific algorithm analyzes the load curve data and identifies the optimal bias voltage (optimal WP), for each NTD.

³The absorber internal gain, in case of cryogenic calorimeters, is considered as the conversion factor from deposited energy to temperature variation. It is inversely proportional to the lattice heat capacity ($C_{lat} \propto T^3$), for a fixed energy release. Therefore, a lower heat capacity C_{lat} , obtained for lower base temperatures, is preferred in order to have a larger signal amplitude.

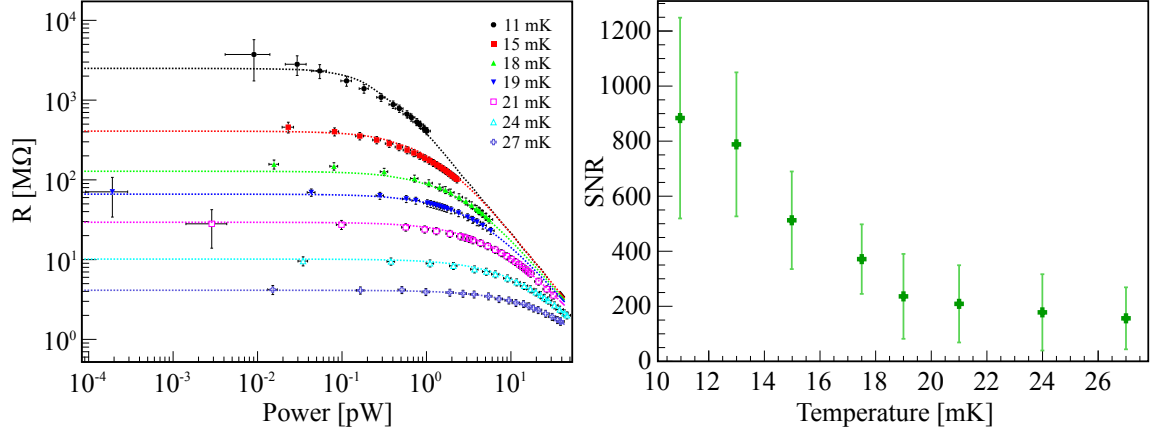


Figure 9. [Left] P-R curves on one CUORE NTD for several values of base temperature, from 11 mK to 27 mK. [Right] Variation of the (average) SNR evaluated over a subset of detectors for several values of base temperature.

Furthermore, the addition of the information related to the pulse shape dependence with the applied bias constitutes an upgrade of the standard approach of choosing optimal WP bias voltages corresponding to either only the maximum amplitude or maximum SNR.

This is the first time that an automatic procedure is utilized for setting the optimal WP for almost one thousand NTDs coupled to TeO₂ crystals and can be reproduced for load curve data acquired at any base temperature. This was crucial to find the best operating settings of the CUORE detector.

Any cryogenic experiment employing macro-calorimeters coupled with NTDs, could profit from the highly automated system presented in this paper, for easing the procedures to optimize the detectors' operating settings.

Acknowledgments

This work was sponsored by the Istituto Nazionale di Fisica Nucleare (INFN). In addition we would like to acknowledge the support from the DOE Office of Science, Office of Nuclear Physics. The authors thank the CUORE Collaboration, the directors and staff of the Laboratori Nazionali del Gran Sasso.

References

- [1] C. Enss and D. McCammon, *Physical principles of low temperature detectors: Ultimate performance limits and current detector capabilities*, *Journal of Low Temperature Physics* **151** (2008) 5–24.
- [2] CUORE collaboration, D. R. Artusa et al., *Searching for neutrinoless double-beta decay of ¹³⁰Te with CUORE*, *Adv. High Energy Phys.* **2015** (2015) 879871, [[1402.6072](#)].
- [3] CUORE collaboration, C. Alduino et al., *CUORE-0 detector: design, construction and operation*, *JINST* **11** (2016) P07009, [[1604.05465](#)].

- [4] E. Andreotti, C. Brofferio, L. Foggetta, A. Giuliani, B. Margesin, C. Nones et al., *Production, characterization, and selection of the heating elements for the response stabilization of the CUORE bolometers*, *Nuclear Instruments and Methods in Physics Research Section A: Accelerators, Spectrometers, Detectors and Associated Equipment* **664** (2012) 161 – 170.
- [5] A. Alessandrello, C. Brofferio, C. Bucci, O. Cremonesi, A. Giuliani, B. Margesin et al., *Methods for response stabilization in bolometers for rare decays*, *Nucl. Instrum. Meth. A* **412** (1998) 454 – 464.
- [6] C. Brofferio and S. Dell’Oro, *Contributed review: The saga of neutrinoless double beta decay search with TeO_2 thermal detectors*, *Review of Scientific Instruments* **89** (2018) 121502, [<https://doi.org/10.1063/1.5031485>].
- [7] CUORE collaboration, I. Nutini et al., *The CUORE Detector and Results*, *J. Low Temp. Phys.* **199** (2020) 519–528.
- [8] C. Alduino et al., *The CUORE cryostat: An infrastructure for rare event searches at millikelvin temperatures*, *Cryogenics* **102** (2019) 9–21, [[1904.05745](https://doi.org/10.1016/j.cryogenics.2019.05.014)].
- [9] A. D’Addabbo, C. Bucci, L. Canonica, S. Di Domizio, P. Gorla, L. Marini et al., *An active noise cancellation technique for the CUORE Pulse Tube Cryocoolers*, *Cryogenics* **93** (2018) 56–65, [[1712.02753](https://doi.org/10.1016/j.cryogenics.2017.12.011)].
- [10] O. Azzolini et al., *CUPID-0: the first array of enriched scintillating bolometers for $0\nu\beta\beta$ decay investigations*, *The European Physical Journal C* **78** (May, 2018) 428, [[1802.06562](https://doi.org/10.1007/s00034-018-0656-2)].
- [11] O. Azzolini et al., *Search for Neutrino-less Double Beta Decay of ^{64}Zn and ^{70}Zn with CUPID-0*, *Phys. Rev. Lett.* **2003**.10840.
- [12] CUORE collaboration, D. Adams et al., *Improved Limit on Neutrinoless Double-Beta Decay in ^{130}Te with CUORE*, *Phys. Rev. Lett.* **124** (2020) 122501, [[1912.10966](https://doi.org/10.1103/PhysRevLett.124.122501)].
- [13] O. Azzolini et al., *Evidence of Single State Dominance in the Two-Neutrino Double- β Decay of ^{82}Se with CUPID-0*, *Phys. Rev. Lett.* **123** (2019) 262501, [[1909.03397](https://doi.org/10.1103/PhysRevLett.123.262501)].
- [14] CUPID collaboration, O. Azzolini et al., *Final result of CUPID-0 phase-I in the search for the ^{82}Se Neutrinoless Double- β Decay*, *Phys. Rev. Lett.* **123** (2019) 032501, [[1906.05001](https://doi.org/10.1103/PhysRevLett.123.032501)].
- [15] CUPID collaboration, O. Azzolini et al., *Search of the neutrino-less double beta decay of ^{82}Se into the excited states of ^{82}Kr with CUPID-0*, *Eur. Phys. J. C* **78** (2018) 888, [[1807.00665](https://doi.org/10.1007/s00034-018-0665-2)].
- [16] O. Azzolini et al., *First Result on the Neutrinoless Double Beta Decay of ^{82}Se with CUPID-0*, *Phys. Rev. Lett.* **1802**.07791.
- [17] CUORE collaboration, C. Alduino et al., *First Results from CUORE: A Search for Lepton Number Violation via $0\nu\beta\beta$ Decay of ^{130}Te* , *Phys. Rev. Lett.* **120** (2018) 132501, [[1710.07988](https://doi.org/10.1103/PhysRevLett.120.132501)].
- [18] CUPID collaboration, W. R. Armstrong et al., *CUPID pre-CDR*, [1907.09376](https://arxiv.org/abs/1907.09376).
- [19] E. E. Haller, N. P. Palaio, M. Rodder, W. L. Hansen and E. Kreysa, *NTD germanium: A novel material for low temperature bolometers*, in *Neutron Transmutation Doping of Semiconductor Materials* (R. D. Larrabee, ed.), pp. 21–36. Springer US, 1984. [DOI](https://doi.org/10.1007/978-1-4613-2500-0_2).
- [20] N. Wang, F. C. Wellstood, B. Sadoulet, E. E. Haller and J. Beeman, *Electrical and thermal properties of neutron-transmutation-doped Ge at 20 mK*, *Phys. Rev. B* **41** (Feb, 1990) 3761–3768.
- [21] N. F. Mott and J. H. Davies, *Metal-insulator transition in doped semiconductors*, *Philos. Mag. B* **42** (1980) 845–858.
- [22] A. Miller and E. Abrahams, *Impurity Conduction at Low Concentrations*, *Phys. Rev.* **120** (1960) 745–755.

- [23] D. McCammon, *Thermal equilibrium calorimeters – an introduction*, in *Cryogenic Particle Detection* (C. Enss, ed.), pp. 1–34. Springer US, 2005. [arXiv:physics/0503045](#).
- [24] C. Arnaboldi, C. Bucci, S. Capelli, P. Gorla, E. Guardincerri, A. Nucciotti et al., *The temperature stabilization system of CUORICINO: An array of macro bolometers*, *Nuclear Science, IEEE Transactions on* **52** (11, 2005) 1630 – 1637.
- [25] C. Arnaboldi, P. Carniti, L. Cassina, C. Gotti, X. Liu, M. Maino et al., *A front-end electronic system for large arrays of bolometers*, *JINST* **13** (2018) P02026, [[1710.06365](#)].
- [26] K. Alfonso, L. Cassina, A. Giachero, C. Gotti, G. Pessina and P. Carniti, *A High Precision Pulse Generation and Stabilization System for Bolometric Experiments*, *JINST* **13** (2018) P02029, [[1710.05565](#)].
- [27] C. Arnaboldi, M. Cariello, S. Di Domizio, A. Giachero and G. Pessina, *A programmable multichannel antialiasing filter for the CUORE experiment*, *Nucl. Instrum. Meth. A* **617** (2010) 327 – 328.
- [28] C. Arnaboldi, A. Bañz, P. Carniti, L. Cassina, A. Giachero, C. Gotti et al., *Very low noise ac/dc power supply systems for large detector arrays*, *Review of Scientific Instruments* **86** (2015) 124703.
- [29] P. Carniti, L. Cassina, C. Gotti, M. Maino and G. Pessina, *A low noise and high precision linear power supply with thermal foldback protection*, *Review of Scientific Instruments* **87** (2016) 054706.
- [30] C. Arnaboldi and G. Pessina, *The design of the input stage for the very front-end of the cuore experiment*, *Journal of Low Temperature Physics* **151** (2008) 964–970.
- [31] A. Alessandrello, C. Brofferio, D. Camin, O. Cremonesi, A. Giuliani, A. Nucciotti et al., *Measuring thermistor resistance with very low d.c. power dissipation*, *Cryogenics* **37** (1997) 27 – 31.
- [32] S. Di Domizio, A. Branca, A. Caminata, L. Canonica, S. Copello, A. Giachero et al., *A data acquisition and control system for large mass bolometer arrays*, *JINST* **13** (2018) P12003, [[1807.11446](#)].
- [33] CUORE collaboration, C. Alduino et al., *Analysis techniques for the evaluation of the neutrinoless double- β decay lifetime in ^{130}Te with the CUORE-0 detector*, *Phys. Rev. C* **93** (2016) 045503, [[1601.01334](#)].
- [34] E. Gatti and P. F. Manfredi, *Processing the Signals From Solid State Detectors in Elementary Particle Physics*, *Riv. Nuovo Cim.* **9N1** (1986) 1–146.
- [35] I. Nutini, *The CUORE experiment: detector optimization and modelling and CPT conservation limit*. PhD thesis, SISSA, Trieste, 2019.